Measurement of $e^+e^- \to K^+K^-K^+K^-$ and ϕK^+K^- from 2.100 to 3.080 GeV

(Dated: November 10, 2017)

Based on data set collected by BESIII detector at BEPCII collider at center of mass energies between 2.100 and 3.080 GeV, Born cross sections of $e^+e^- \to K^+K^-K^+K^-$ and $e^+e^- \to \phi K^+K^-$ have been measured precisely. The BESIII's results are consistent with BABAR's results for $K^+K^-K^+K^-$. The energy dependence of $K^+K^-K^+K^-$ and ϕK^+K^- cross sections differs significantly from that of $e^+e^- \to \phi\pi^+\pi^-$. There is an enhancement around 2.232 GeV. Born cross section at $\sqrt{s} = 2.2324$ GeV differs by about 4.6 s.d. and 7.3 s.d. with respect to the closest measurements for ϕK^+K^- and $K^+K^-K^+K^-$, respectively.

PACS numbers: 13.25.Gv, 12.38.Qk, 14.20.Gk, 14.40.Cs

I. INTRODUCTION

The $\phi(2170)$, denoted previously as Y(2175), was firstly observed in the initial state radiation method with $e^+e^- \to \phi f_0(980)$ [1]. It was confirmed by BESII [2], BESIII [3] and Belle [4]. The charmoniumlike vector state has been observed with $e^+e^- \to K^+K^-J/\psi$ [5] above the $D\bar{D}$ production threshold. The $s\bar{s}$ bound states are of interest, but they are much less known compared to $c\bar{c}$. A similar decay mode, $e^+e^- \to \phi K^+K^-$, provides a good opportunity to study charmoniumlike vector states below the $D\bar{D}$ production threshold.

The theorists explained $\phi(2170)$ as a $s\bar{s}g$ hybrid [6], a 2^3D_1 $s\bar{s}$ [7], a tetraquark state [8, 9], a $\Lambda\bar{\Lambda}$ bound state [10]. The 1^{--} $s\bar{s}g$ hybrid can decay to $\phi\pi\pi$, with cascade ($s\bar{s} \to (s\bar{s})(gg) \to \phi\pi\pi$) [11], and $s\bar{s}g \to \phi f_0(980)$ may make a significant contribution. Because $f_0(980)/a_0(980)$ have been observed [12], it is useful to study $\phi f_0(980)/a_0(980)$ within $K^+K^-K^+K^-$ final state. The Ref. [13] used Faddeev calculation for three body interaction of ϕK^+K^-, obtained a peak around 2.150 GeV and in the invariant mass of K^+K^- system around 970 MeV. It also stimulates experimentalists to study energy dependence of ϕK^+K^- and $K^+K^-K^+K^-$.

BABAR Collaboration has measured the cross sections of $e^+e^- \to K^+K^-K^+K^-$ and observed an enhancement around 2.3 GeV [14, 15]. However, there are no published electron-positron data for comparison. There are ϕ, $f_0(1370)$ and $f_2'(1525)$ on invariant mass of K^+K^- pair and BABAR also observed bump or broad structure around 2.175 GeV and 2.7 GeV, which is need for further study.

BESIII Collaboration collected about 650 pb^{-1} data between 2.0 GeV and 3.08 GeV, the $e^+e^- \to K^+K^-K^+K^-$ could be measured, and compared with BABAR's results. This paper presents the study of $e^+e^- \to K^+K^-K^+K^-$. The $e^+e^- \to \phi K^+K^-$, the dominant intermediate process of $K^+K^-K^+K^-$ is also reported.

II. DETECTOR AND DATA SAMPLES

BEPCII [17] is a double-ring e^+e^- collider running at center-of-mass (CM) energies ranging from 2.0 to 4.6 GeV, and providing a peak luminosity of 1.0×10^{33} cm^{-2}s^{-1} at the CM energy of 3.770 GeV. The BESIII [17] detector has a geometrical acceptance of 93% of 4π and has four main components: (1) A small-cell, helium-based (60% He, 40% C_3H_8) main drift chamber (MDC) with 43 layers providing an average single-hit resolution of 135 μm, and a charged-particle momentum resolution in a 1 T magnetic field of 0.5% at 1 GeV/c. (2) An electromagnetic calorimeter (EMC) consisting of 6240 CsI(Tl) crystals in a cylindrical structure (barrel) and two endcaps. The energy resolution at 1.0 GeV/c is 2.5% (5%) in the barrel (endcaps), and the position resolution is 6 mm (9 mm) in the barrel (endcaps). (3) Particle Identification is provided by a time-of-flight system (TOF) constructed of 5-cm-thick plastic scintillators, with 176 detectors of 2.4 m length in two layers in the barrel and 96 fan-shaped detectors in the endcaps. The barrel (endcap) time resolution of 80 ps (110 ps) provides 2σ K/π separation for momenta up to ~ 1.0 GeV/c. (4) The muon system (MUC) consists of 1000 m^2 of Resistive Plate Chambers (RPCs) in nine barrel and eight endcap layers and provides 2 cm position resolution.

The optimization of selection criteria, determination of detection efficiencies and estimations of potential backgrounds are performed based on Monte Carlo (MC) simulations taking various aspects of the experimental setup into account. Geant4-based MC simulation software, which includes geometric and material description of the BESIII detector, detector response and digitization models, as well accounting of the detector running conditions and performances, is used to generate MC samples.

The signal $e^+e^- \to K^+K^-K^+K^-$ and $e^+e^- \to \phi K^+K^-$ are simulated with ConExc generator [19], in order to study contribution of background events, MC samples of $e^+e^- \to e^+e^-$ and $\mu^+\mu^-$ are generated with Babayaga 3.5 [18]. $e^+e^- \to q\bar{q}$ process is simulated with ConExc generator [19].

III. EVENT SELECTION

The final states of $e^+e^- \rightarrow K^+K^-K^+K^-$ and $e^+e^- \rightarrow \phi K^+K^-$ ($\phi \rightarrow K^+K^-$) have four kaons. Because center-of-mass of data set is close to threshold of four kaons, the kaon has small momentum. In order to increase event selection efficiency, the candidate events are required to have at least three charged tracks.

Charged tracks are reconstructed from hits in the MDC. Each charged track is required to have a polar angle that is well within fiducial volume of the MDC, $|cos\theta| < 0.93$, where θ is polar angle of track in laboratory frame, to have a point of closest approach to interaction point that is within ± 10 cm along beam direction and within 1 cm in radial direction. For each charged track, the TOF information and dE/dx information are combined to form particle identification (PID) confidence levels for π, K, p hypotheses, and particle type with the highest probability is assigned to each track. In order to reconstruct the primary vertex, vertex fit is applied for vertex with three kaons.

In analysis of $e^+e^- \rightarrow K^+K^-K^+K^-$, if event has four identified kaons , combination with the least $\chi^2_{vertexfit}$ is retained. Fig. 1 (left) shows the plot of momentum of three identified kaons, where black dots are experimental data. The peak around $\sqrt{s}/2$ results from $e^+e^- \rightarrow e^+e^-$ and $e^+e^- \rightarrow \mu^+\mu^-$. In order to reduce these background events, the momentum of identified particles is required to be less than $0.8 * p_{Beam}$. Fig. 1 (right) represents the comparison within the requirement of the momentum.

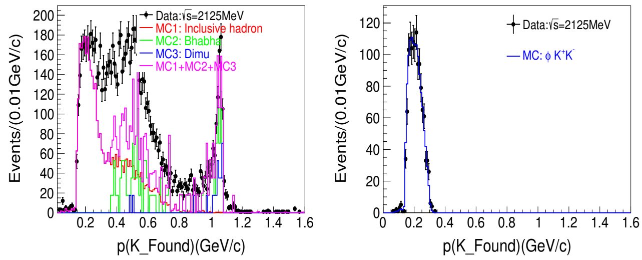

FIG. 1: (color online) Momentum distributions of three identified kaons at 2.125 GeV. Left plot: The black dots with error bar are experimental data events, red histogram is from inclusive MC samples, green histogram is from bhabha MC samples, the blue histogram is from Dimu MC samples, the light red histogram is the sum of all MC samples. Right plot: After cutting momentum, imomentum distribution of recoiling Kaons at 2.125 GeV. Here, the black dots with error bar are experimental data events and blue histogram is from MC samples: ϕ K^+K^-.

For $e^+e^- \rightarrow \phi K^+K^-$, where ϕ is reconstructed with K^+ and K^-. a one constraint (1C) kinematic fit is performed under the hypothesis that the KK^+K^- missing mass corresponds to the kaon mass. As for events have identified four kaons , the combination with the least χ^2_{1C} has been chosen. The chi-square of the kinematic fit, χ^2_{1C}, is required to be less than 20, which is optimatized with $S/\sqrt{S+B}$. Fig. 2 shows M(K^+K^-) distribution from experimental data samples at 3.080 GeV, it indicates that $e^+e^- \rightarrow \phi$ K^+K^- dominants $K^+K^-K^+K^-$ final states, where the black dots with error bar are the best ϕ candidates space(closest to the ϕ-meson mass) and blue histogram is filled by four entries, which is the different combination from all K^+K^- pairs. The ϕ signal is observed clearly with very low background.

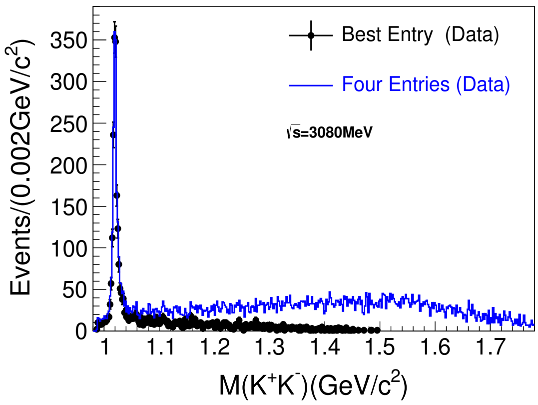

FIG. 2: (color online) (a) M(K^+K^-) distributions: the black dots with error bar are the best ϕ candidates(closest to the $\phi - meson$ mass) and blue histogram is filled by four entries, which is the different combination from mass(K^+K^-).

IV. DETECTION EFFICIENCIES

The $e^+e^- \rightarrow \phi K^+K^-$ is simulated by phase space model (PHSP) for three body decay. However, the PHSP MC could not describe experimental data, as shown in Fig. 3 (b), where the background contributions are estimated with events from ϕ sideband region in Fig. 3 (a). We use partial wave analysis (PWA) method to calculate MC efficiency from different modes include intermediate resonances at the 3.08 GeV, and find they give similar results. To obtain a much more reliable MC description, the method of event-by-event weight is applied for invariant mass distribution of K^+K^- in Fig. 4 (a), where weighting factors are ratio of event number between experimental data and MC data bin-by-bin. Comparison of invariant mass distribution of $\phi K^\pm$ is shown in Fig. 4(b).

Although $e^+e^- \rightarrow \phi K^+K^-$ includes intermediate resonance, the difference of MC efficiency for $e^+e^- \rightarrow K^+K^-K^+K^-$ (PHSP) is less than 3%. The weighted MC efficiency is used as signal efficiency of final states of $K^+K^-K^+K^-$ including ϕ resonance. Figure. 5 shows comparison of the momentum distributions of kaon between experimental data and weighted MC.

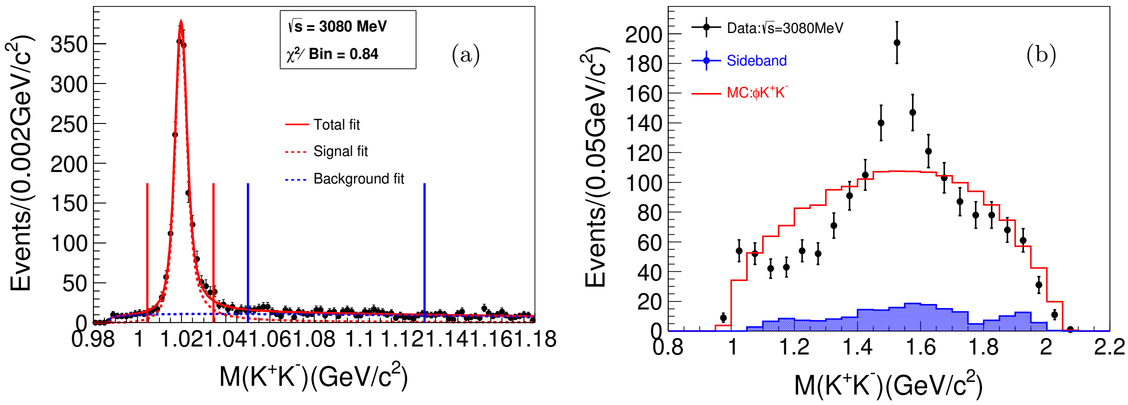

FIG. 3: (a) Fit to invariant mass distribution of K^+K^- at 3.080 GeV, K^+K^- is from ϕ. The red solid curve is total fit, the dashed red line describes signal and the blue dashed curve is background. (b) Invariant mass distribution of K^+K^-, K^+K^- is not from ϕ. The blue histogram is from sideband region and the red histogram is signal MC samples of $e^+e^- \to \phi\ K^+K^-$. Here, the black dots with error bar are experimental data events.

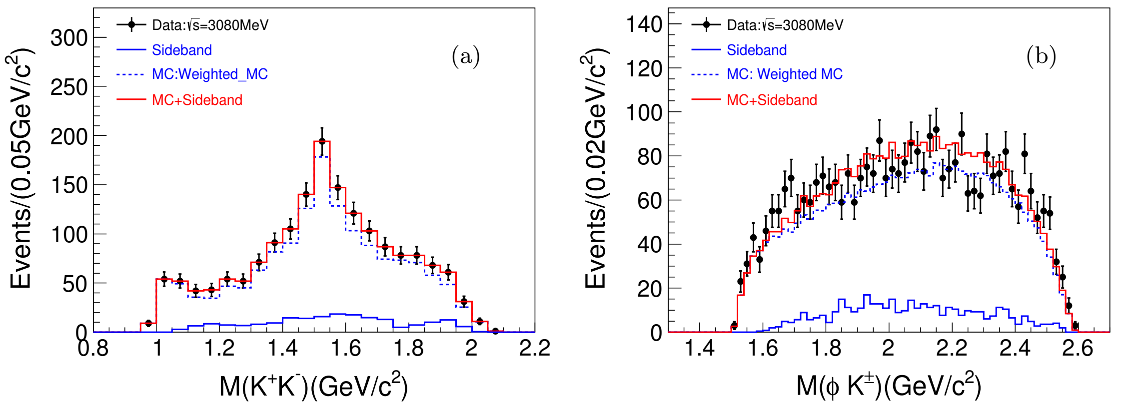

FIG. 4: (color online). (a) Invariant mass distribution of K^+K^- at 3.080 GeV, K^+K^- is not from ϕ. (b) Invariant mass distribution of $(\phi K^{\pm})$ at 3.080 GeV. Here, the black dots with error bar are experimental data events, the blue histograms are from sideband region, the dashed blue histograms are from weighted MC and the red histograms represent the sum of sideband events and the weighted MC.

V. EXTRACTION OF THE BORN CROSS SECTION

The Born cross section is determined from

$$\sigma^B = \frac{N^{obs}}{\mathcal{L}_{int} \cdot (1+\delta) \cdot \epsilon \cdot \mathcal{B}}, \tag{1}$$

where N^{obs} is the number of observed signal events, $\mathcal{L}_{int}$ is integrated luminosity, $(1+\delta)$ stands for $(1+\delta^r)\cdot(1+\delta^v)$. $(1+\delta^r)$ is the ISR correction factor which is obtained by QED calculation [20] and taking the cross section measured in this analysis after iterations as input. $(1+\delta^v)$ is vacuum polarization (VP) factor, which is taken from QED calculation [21], ϵ is event selection efficiency, $\mathcal{B}$ is branching ratio, $\mathcal{B}(\phi \to K^+K^-) = 48.9\%$, taken from the Particle Data Group (PDG) [12].

The event number of $e^+e^- \to K^+K^-K^+K^-$ is obtained by fitting on recoil mass of three kaon system, which is shown in Fig. 6 for $\sqrt{s} = 3.08$ GeV. According to background study of $e^+e^- \to q\bar{q}$ MC, there is no peaking background. The unbinned maximum likelihood method is also performed. The signal is described with the $e^+e^- \to K^+K^-K^+K^-$ MC shape convoluted with a Gaussian function which discribes the difference of mass resolution between MC and experimental data and the Chebychev polynominal function describes contribution from background event, which is confirmed in background study. Table I summarizes L_{int}, N^{obs}, $(1+\delta)$ and ϵ in Eq. 1. The measured cross section is also included

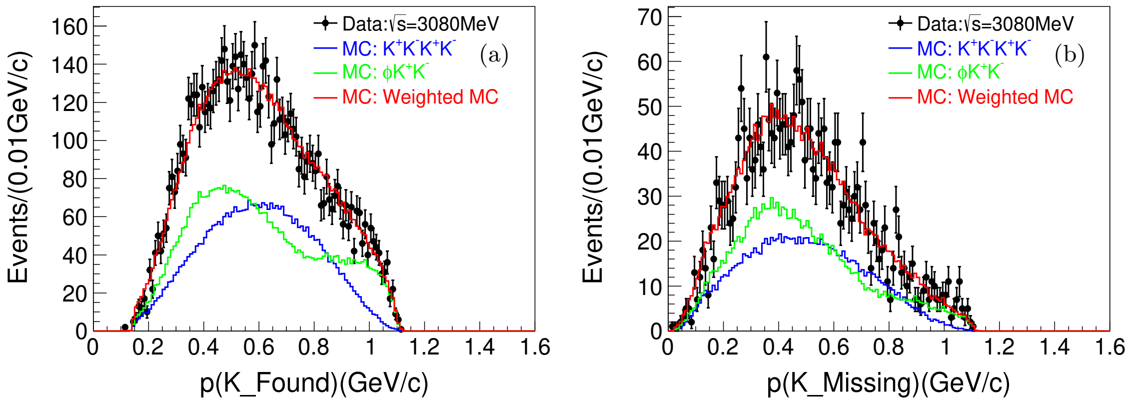

FIG. 5: (color online). Momentum distributions of three identified kaons (a) and the recoiling kaons (b). Here, the black dots with error bar are experimental data events, blue histograms are from signal MC samples $e^+e^- \to K^+K^-K^+K^-$, green histograms are from signal MC samples $e^+e^- \to \phi K^+K^-$ and the red histograms are from weighted MC samples of ϕK^+K^- and $K^+K^-K^+K^-$.

for each energy point.

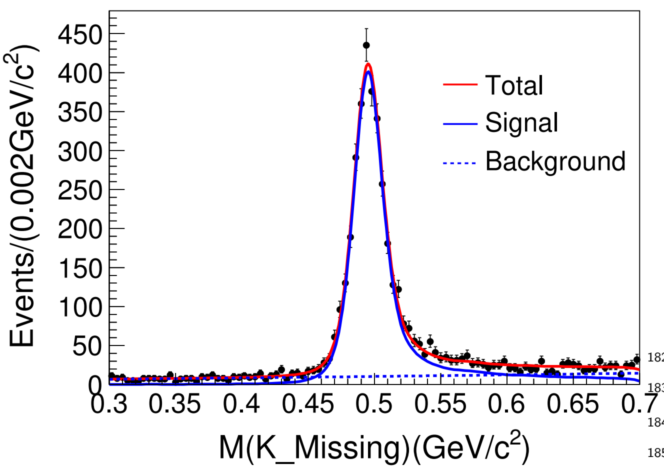

FIG. 6: (color online). Fit to $M(K^+K^-)$ distribution at 3.08 GeV: the black dots with error bar are experimental data, the red solid curve is total fit and the blue dashed curve is background.

The signal yields of $e^+e^- \to \phi K^+K^-$ are obtained by fitting on $M(K^+K^-)$ mass spectra (4 entries per event). The ϕ signal is described by a P-wave Breit-Wigner function (parameters are fixed to PDG values [12]) convoluted with a Gaussian function, which accounts for the difference of mass resolution between the data and the Breit-Wigner function, where the P-wave Breit-Wigner function is defined as

$$f(m) = |\mathrm{A}(m)|^2 \cdot p \tag{2}$$

$$\mathrm{A}(m) = \frac{p_{\phi\to\mathrm{K^+K^-}}^{\mathrm{L}_{\phi\to\mathrm{K^+K^-}}}}{m^2 - m_0^2 + im\Gamma(m)} \cdot \frac{\mathrm{B}(p_{\phi\to\mathrm{K^+K^-}})}{\mathrm{B}(p'_{\phi\to\mathrm{K^+K^-}})} \tag{3}$$

$$\mathrm{B}(p, \mathrm{L}_{\phi\to\mathrm{K^+K^-}} = 1, \mathrm{R} = 3\mathrm{G}e\mathrm{V}) = \frac{1}{\sqrt{1 + (\mathrm{R}p)^2}} \tag{4}$$

$$\Gamma(m) = \left(\frac{p}{p'}\right)^{2\mathrm{L}_{\phi\to\mathrm{K^+K^-}}+1}\left(\frac{m_0}{m}\right)\Gamma_0\left[\frac{\mathrm{B}(p)}{\mathrm{B}(p')}\right] \tag{5}$$

where m_0 is nominal mass of ϕ as specified in PDG 2016 [12] and p is momentum of kaon in the frame of ϕ for $\sqrt{s}$. p' is the same, but for the nominal mass of ϕ. Here, Γ_0 is the mass width of ϕ. The angular momentum (L) is equal to be 1, which is assumed to be the lowest allowed given the parent and daughter spins. $B(p)$ is the Blatt-Wdisskopf form factor [22], which depends on L. R is 3 GeV^{-1}.

The background shape is parametrized with an ARGUS function [23]. The parameters of the Gaussian function and the ARGUS function are free parameters in the fit. The corresponding fit result for $\sqrt{s} = 3.08$ GeV is shown in Figure 7. Table II summarizes L_{int}, N^{obs}, $(1+\delta)$, ϵ and Born cross section in Eq. 1.

Here, the initial input cross section is from $K^+K^-K^+K^-$ final state, which is the result from BABAR Collaboration [15]. Then the line shape of the production cross section used as input in ConExc generator is obtained as following:

- Step 1: measure the observed cross sections from 2.10 to 3.08 GeV using BESIII data samples at 20 CM energies.

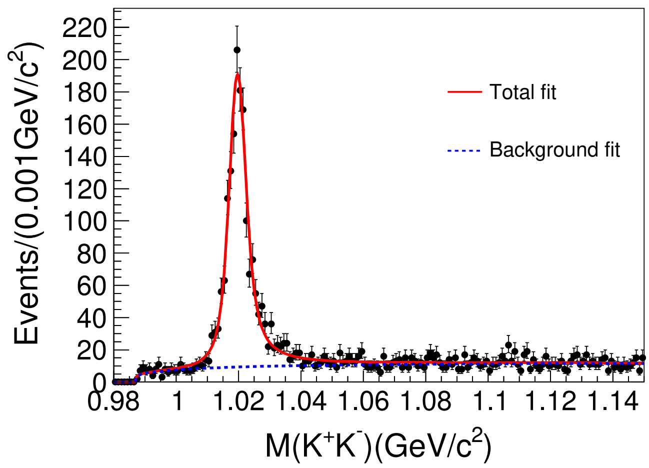

FIG. 7: (color online). Fit of $M(K^+K^-)$ distribution at 3.08 GeV: the black dots with error bar are experimental data, the red solid curve is total fit and the blue dashed curve is background.

- Step 2: the cross section from step 1 are parameterized with incoherent sum of Breit-Wigner (BW) functions and polynomial functions, and the fitted results are used as generator input.
- Step 3: generate MC events with the input lineshape, and the ISR factor is calculated by the generator for users, we can find details of calculation in appendix C.12.
- Step 4: iterate above threes steps until a stable result is obtained , the criteria is to require the difference of cross sections in two convergent iteration less than 1.0%.

By iterating a few times, the values of ISR and efficiency become stable, then we can get convergent cross section of $e^+e^- \to K^+K^-K^+K^-$ and $e^+e^- \to \phi K^+K^-$.

VI. SYSTEMATIC UNCERTAINTY

Systematic uncertainties in measurement of Born cross sections of $e^+e^- \to \phi K^+K^-$ include luminosity measurements, differences between experimental data and MC simulation for tracking and PID efficiency, kinematic fit, fit procedure, MC simulation of ISR correction factor and vacuum polarization factor, as well as uncertainties in branching fractions of intermediate state decays.

(a) *Luminosity:* The integrated luminosity of the data set are measured with large angle Bhabha events, and corresponding uncertainties are estimated to be 1.0% [24].

TABLE I: Cross section of $e^+e^- \to K^+K^-K^+K^-$. The table shows the c.m. energy $\sqrt{s}$, integrated luminosity L_{int}, number of final states including $K^+K^-K^+K^-$ events N^{obs}, $(1+\delta)$ represents radiative correction factor and vacuum polarization factor, Born cross section σ^B. The first uncertainties are statistical and the second systematic.

$\sqrt{s}$ (GeV)	L_{int} (pb^{-1})	N^{obs}	$(1+\delta)$	$\epsilon(\%)$	σ (pb)(stat±sys)
3.080	126.19	3693.7±73.1	1.0185	61.91	46.4±0.9±2.6
3.020	17.29	591.4±29.2	1.0854	63.28	49.8±2.5±3.0
3.000	15.88	557.3±28.1	1.0860	63.31	51.0±2.6±2.9
2.981	16.07	555.6±28.1	1.0846	63.57	50.1±2.5±3.0
2.950	15.94	629.1±29.5	1.0799	63.14	57.9±2.7±3.4
2.900	105.25	4366.4±76.1	1.0686	63.98	60.7±1.1±3.5
2.800	1.01	37.25±7.3	1.0424	64.45	54.9±10.8±3.9
2.700	1.03	44.2±7.3	1.0173	62.65	50.2±10.8±4.7
2.646	34.00	1817.6±47.1	1.0049	61.25	86.8±2.3±4.9
2.644	33.72	1819.9±47.0	1.0044	61.43	87.5±2.3±5.0
2.500	1.10	55.3±8.0	0.9741	57.35	90.2±13.0±10.6
2.396	66.87	2838.7±57.4	0.9534	50.00	89.0±1.8±7.5
2.386	22.55	934.6±32.0	0.9515	46.10	94.5±3.2±5.5
2.309	21.09	682.3±28.0	0.9488	42.33	81.4±3.3±6.2
2.232	11.86	369.2±19.8	0.8505	30.99	110.0±5.9±6.3
2.200	13.70	206.6±15.3	0.8824	27.58	62.0±4.6±5.9
2.175	10.63	95.6±9.9	0.8750	23.24	44.2±4.6±4.2
2.150	2.84	17.8±3.9	0.8616	17.45	41.7±9.1±4.8
2.125	108.49	378.7±19.3	0.8437	12.24	33.8±1.7±4.2
2.100	12.17	18.9±8.8	0.8186	7.18	26.4±12.3±3.7

TABLE II: Cross section of $e^+e^- \to \phi K^+K^-$. The table shows the c.m. energy $\sqrt{s}$, integrated luminosity L_{int}, number of observed ϕ events N^{obs}, $(1+\delta)$ represents radiative correction factor and vacuum polarization factor, Born cross section σ^B. The first uncertainties are statistical and the second systematic.

$\sqrt{s}$ (GeV)	L_{int} (pb^{-1})	N^{obs}	$(1+\delta)$	$\epsilon(\%)$	σ^B (pb)(stat±sys)
3.080	126.19	1690.8±50.1	1.0065	49.7	54.8±1.6±3.3
3.020	17.29	253.7±19.9	1.0996	50.2	54.4±4.3±3.8
3.000	15.88	242.6±18.8	1.1064	50.0	56.5±4.4±4.0
2.981	16.07	245.9±20.0	1.1098	49.5	57.0±4.6±3.6
2.950	15.94	282.2±20.4	1.1099	48.6	67.1±4.9±4.3
2.900	105.25	2010.8±54.4	1.1013	49.2	72.1±2.0±4.6
2.800	1.01	13.2±4.5	1.0702	47.9	52.2±17.8±4.9
2.700	1.03	26.0±6.1	1.0376	48.8	101.6±23.8±10.2
2.646	34.00	901.3±37.7	1.0217	46.5	114.1±4.8±7.5
2.644	33.72	883.1±37.5	1.0211	46.4	113.0±4.8±8.0
2.500	1.10	25.5±6.9	0.9846	43.4	111.1±30.1±10.7
2.396	66.87	1841.6±56.2	0.9618	38.2	153.3±4.7±13.0
2.386	22.55	573.4±31.6	0.9598	37.4	144.9±8.0±14.5
2.309	21.09	377.0±26.0	0.9465	32.6	118.5±8.2±9.2
2.232	11.86	260.0±22.3	0.8543	27.2	193.0±16.6±16.6
2.200	13.70	137.7±18.7	0.8898	21.7	106.5±14.5±8.7
2.175	10.62	84.5±15.6	0.8835	18.8	97.9±18.1±7.6
2.150	2.84	15.8±5.9	0.8714	13.7	95.3±35.6±15.2
2.125	108.49	309.6±31.5	0.8555	9.6	71.1±7.2±5.4
2.100	12.17	12.9±6.1	0.8346	5.7	45.6±21.6±8.4

(b) *Tracking:* The tracking efficiency uncertainty is estimated to be 1.0% [25] for each track with control sample $e^+e^- \to K^+K^-\pi^+\pi^-$. The 3.0% is taken as the systematic uncertainty of tracking efficiency.

(c) *PID:* To estimate the PID efficiency uncertainty, we study $K^\pm$ PID efficiencies with the same control samples $e^+e^- \to K^+K^-\pi^+\pi^-$. The average PID efficiency difference between data and MC is found to be 1.5 % per charged track and taken as a systematic uncertainty. The 4.5% is taken as the systematic uncertainty on PID efficiency.

(d) *Kinematic fit:* The uncertainty from the 1C kinematic fit is estimated by correcting the simulated track helix parameters (ϕ_0, κ, $tan\lambda$), where ϕ_0 is azimuthal angle that specifies the pivot with respect to the helix center, κ is the reciprocal of the transverse momentum and $tan\lambda$ is the slope of the track. The correction factors are quoted from Ref. [26]. The difference in this efficiency from its nominal value is taken to be the uncertainty.

(e) *Fitting procedure:* The following three aspects are considered for fit procedure. (1) *Fitting range:* In fit, the $M(K^+K^-)$ is fitted in a region from 0.98 to 1.15 GeV/c^2. An alternative fit with fit range between 0.98 and 1.20 GeV/c^2 is performed. The $M(K^{\pm})$ of the recoiled kaon is fitted by varying from (0.3, 0.7) GeV/c^2 to (0.31, 0.69) GeV/c^2. (2) *Signal shape:* The signal shape of the ϕ is described by a P-wave BW function convoluted with a Gaussian function. An alternative fit with a MC shape convoluted with a Gaussian function is performed. The signal shape of recoiled kaon is described by MC shape convoluted with a Gaussian function. The uncertainty related with the signal line shape is estimated with an alternative fit with the same function for signal line-shape, but fixing width of Gaussian function to the value by changing one standard deviation of width obtained in the nominal fit. The difference in the yield with respect to the nominal fit is considered as the systematic uncertainty from the signal shape. (3) *Background shape:* Background shapes for ϕ are described as a Argus function. The fit with a second-order polynomial function for the background shape is used to estimate its uncertainty. The background shapes for recoiled kaon are described as a Chebychev polynomial function. The fit with a first-order Chebychev polynomial function for the background shape is used to estimate its uncertainty. (f) *ISR factor:* Uncertainties in the initial cross section line shape used in generator introduce systematic uncertainties in the radiative correction factor and the efficiency. This is estimated using difference between the last two iterations.

(g) *VP factor:* The uncertainty is estimated to be 0.5 % [21].

(h) *Branching fraction:* The experimental uncertainties in the branching fractions for the processes $\phi \to K^+K^-$) are taken from the PDG [12].

(i) *Efficiency:* To obtain signal efficiency properly, the method of event-by-event weight is applied. We weight the MC to the data by M(K^+K^-) weight factor , which the weight factor histogram is obtained by calculating the ratio of the number of signal events from data and MC bin-by-bin. Then the weighted MC distributions are consistent well with the data. The difference of efficiency between $e^+e^- \to \phi K^+K^-$ and weighted MC is worked as uncertainty. For the process of final states including four kaons, the difference of branch ratio between $e^+e^- \to \phi K^+K^-$ and $e^+e^- \to K^+K^-K^+K^-$ from PHSP is worked as systematic uncertainty

(j) *MC:* Signal efficiency is determined with MC simulation samples, whose statistics introduces an uncertainty as described with the following formula.

(k) *Other systematic uncertainties:* Other sources of systematic uncertainties include the trigger efficiency, event start time determination and final-state-radiation simulation. The total systematic uncertainty due to these sources is estimated to be less than 1.0%. To be conservative, we take 1.0% as the systematic uncertainty.

Assuming all the sources of systematic uncertainty are independent, the total systematic uncertainties are obtained by adding them in quadrature, which are shown in Tables IV, III.

VII. SUMMARY AND DISCUSSION

We measured Born cross sections for $e^+e^- \to K^+K^-K^+K^-$ at 20 energy points, which is shown in Fig. 8 (a). The results have much better precision at most of energy points than that of BABAR Collaboration. There is a similar bump observed at $\sqrt{s}$ = 2.232 GeV.

The Born cross sections of $e^+e^- \to \phi K^+K^-$ are obtained first time at 20 energy points. Figure 8 (b) shows the cross section line shape of $e^+e^- \to \phi K^+K^-$. By examining the ϕK^+K^- cross section as a function of center of mass energy, there is a bump at $\sqrt{s}$ = 2.2324 GeV. Although BABAR Collaboration have not measured the cross section of $e^+e^- \to \phi K^+K^-$, an enhancement in the cross section of $e^+e^- \to \phi f_0(980)$ and $f_0(980) \to K^+K^-$ is also observed by BABAR Collaboration [15].

Some theorists obtain a neat resonance peak around a total mass of 2150 MeV and an invariant mass for the $K\bar{K}$ system around 970 MeV, which is regarded as $f_0(980)$ in Ref. [13]. However, we observe an enhancement near threshold in the line shape of cross section of $e^+e^- \to \phi K^+K^-$ and $e^+e^- \to K^+K^-K^+K^-$. The result of $e^+e^- \to K^+K^-K^+K^-$ is consistent with BABAR Collaboration. Due to only one energy point around 2.232 GeV, we are not sure that this is resonant structure from $Y(2175)$.

VIII. ACKNOWLEDGMENTS

Acknowledgement The BESIII collaboration thanks the staff of BEPCII and the IHEP computing center and the supercomputing center of USTC for their strong support. This work is supported in part by National

TABLE III: Summary of systematic uncertainties (%) in the cross section of $e^+e^- \to K^+K^-K^+K^-$ for energies. The common uncertainties include luminosity, tracking, branching fraction and others.

$\sqrt{s}$ (GeV)	Luminosity	Tracking	PID	Fitting range	Signal shape	Background shape	ISR	VP	Efficiency	MC	Others	Total
3.080	1.0	3.0	4.5	0.8	0.3	0.1	0.0	0.5	0.1	0.2	1.0	5.7
3.020	1.0	3.0	4.5	1.9	0.8	1.1	0.0	0.5	0.1	0.2	1.0	6.1
3.000	1.0	3.0	4.5	0.4	0.7	0.4	0.2	0.5	0.1	0.2	1.0	5.7
2.981	1.0	3.0	4.5	0.2	0.7	1.6	0.1	0.5	0.1	0.2	1.0	5.9
2.950	1.0	3.0	4.5	0.9	0.4	0.8	0.3	0.5	0.1	0.2	1.0	5.8
2.900	1.0	3.0	4.5	0.4	0.2	0.5	0.0	0.5	0.1	0.2	1.0	5.7
2.800	1.0	3.0	4.5	1.1	1.9	3.8	0.3	0.5	0.5	0.2	1.0	7.1
2.700	1.0	3.0	4.5	0.2	0.2	7.5	0.3	0.5	0.6	0.2	1.0	9.4
2.646	1.0	3.0	4.5	0.0	0.1	0.2	0.5	0.5	0.1	0.2	1.0	5.6
2.644	1.0	3.0	4.5	0.3	0.1	0.7	0.1	0.5	0.1	0.2	1.0	5.7
2.500	1.0	3.0	4.5	7.1	6.9	2.7	0.3	0.5	0.7	0.3	1.0	11.7
2.396	1.0	3.0	4.5	3.5	3.5	3.8	0.4	0.5	0.1	0.3	1.0	8.4
2.386	1.0	3.0	4.5	0.2	0.0	1.2	0.0	0.5	0.7	0.3	1.0	5.8
2.309	1.0	3.0	4.5	1.4	2.1	4.5	0.4	0.5	0.3	0.4	1.0	7.6
2.232	1.0	3.0	4.5	0.7	0.1	0.6	0.4	0.5	0.5	0.5	1.0	5.7
2.200	1.0	3.0	4.5	0.1	0.6	7.6	0.5	0.5	0.5	0.5	1.0	9.5
2.175	1.0	3.0	4.5	1.9	7.3	0.3	0.3	0.5	0.5	0.6	1.0	9.4
2.150	1.0	3.0	4.5	6.7	1.1	7.3	0.7	0.5	0.2	0.7	1.0	11.5
2.125	1.0	3.0	4.5	6.2	1.9	8.8	0.1	0.5	0.2	0.8	1.0	12.3
2.100	1.0	3.0	4.5	3.2	11.6	3.2	0.1	0.5	2.2	1.1	1.0	13.9

TABLE IV: Summary of systematic uncertainties (%) in the cross section of $e^+e^- \to \phi K^+K^-$ for energies. The common uncertainties include luminosity, tracking, branching fraction and others.

$\sqrt{s}$ (GeV)	Luminosity	Tracking	PID	Kinematic fit	Signal shape	Background shape	Fitting range	ISR	VP	Efficiency	MC	Branching fraction	Others	Total
3.080	1.0	3.0	4.5	1.3	0.7	0.0	1.2	0.3	0.5	1.1	0.3	1.1	1.0	6.1
3.020	1.0	3.0	4.5	1.4	2.7	0.8	0.8	0.2	0.5	2.0	0.3	1.1	1.0	6.9
3.000	1.0	3.0	4.5	1.4	0.4	1.3	3.0	0.1	0.5	2.1	0.3	1.1	1.0	7.1
2.981	1.0	3.0	4.5	1.4	1.7	0.4	1.3	0.2	0.5	1.0	0.3	1.1	1.0	6.4
2.950	1.0	3.0	4.5	1.3	2.2	0.3	0.7	0.1	0.5	0.8	0.3	1.1	1.0	6.4
2.900	1.0	3.0	4.5	1.5	2.2	0.1	0.1	0.4	0.5	1.2	0.3	1.1	1.0	6.4
2.800	1.0	3.0	4.5	1.5	7.1	0.0	0.0	0.0	0.5	1.1	0.3	1.1	1.0	9.3
2.700	1.0	3.0	4.5	1.6	7.7	0.0	0.0	0.0	0.5	2.4	0.3	1.1	1.0	10.0
2.646	1.0	3.0	4.5	1.6	2.5	0.5	0.9	0.7	0.5	0.4	0.3	1.1	1.0	6.6
2.644	1.0	3.0	4.5	1.6	2.5	1.9	2.1	0.3	0.5	0.3	0.3	1.1	1.0	7.1
2.500	1.0	3.0	4.5	1.7	6.7	0.0	3.3	0.1	0.5	0.4	0.4	1.1	1.0	9.6
2.396	1.0	3.0	4.5	1.7	5.6	0.1	1.6	0.0	0.5	1.4	0.4	1.1	1.0	8.5
2.386	1.0	3.0	4.5	2.0	7.3	0.9	2.1	0.1	0.5	2.0	0.4	1.1	1.0	10.0
2.309	1.0	3.0	4.5	2.3	2.5	0.8	1.0	0.1	0.5	3.8	0.5	1.1	1.0	7.8
2.232	1.0	3.0	4.5	2.4	5.2	0.4	0.0	0.5	0.5	2.8	0.5	1.1	1.0	8.6
2.200	1.0	3.0	4.5	2.4	3.6	2.2	2.9	0.3	0.5	1.4	0.6	1.1	1.0	8.2
2.175	1.0	3.0	4.5	2.2	2.2	1.2	2.2	0.2	0.5	3.5	0.7	1.1	1.0	7.8
2.150	1.0	3.0	4.5	2.5	12.0	5.9	5.9	0.7	0.5	0.7	0.8	1.1	1.0	15.9
2.125	1.0	3.0	4.5	2.1	0.0	2.8	3.4	0.9	0.5	0.2	1.0	1.1	1.0	7.6
2.100	1.0	3.0	4.5	2.0	7.7	0.0	15.4	1.3	0.5	1.0	1.3	1.1	1.0	18.4

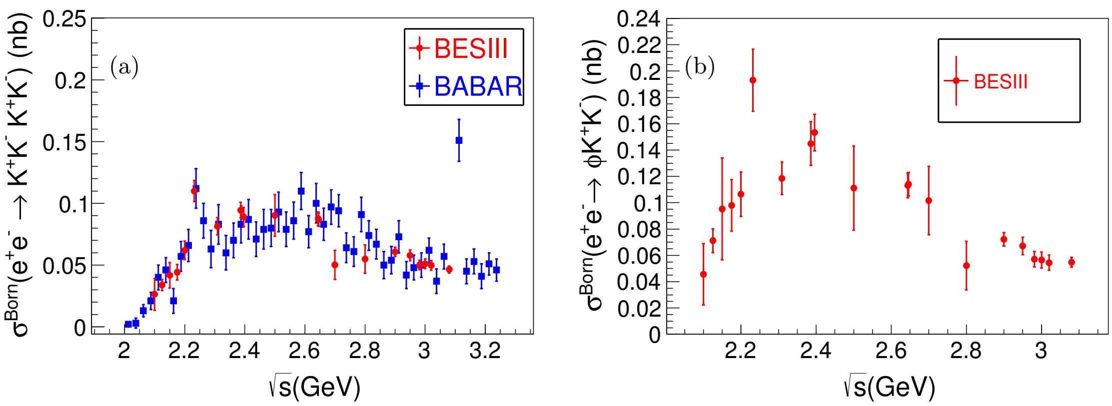

FIG. 8: (color online). (a) The comparison on cross section of $e^+e^- \to K^+K^-K^+K^-$ between BABAR and this work. The blue rectangles with error bars result from BABAR experiment [15], the red dots with error bars result from this work. (b) The cross section line shape of $e^+e^- \to \phi K^+K^-$ obtained in this work.

Key Basic Research Program of China under Contract No. 2015CB856700; National Natural Science Foundation of China (NSFC) under Contracts Nos. 11235011, 11335008, 11425524, 11625523, 11635010; the Chinese Academy of Sciences (CAS) Large-Scale Scientific Facility Program; the CAS Center for Excellence in Particle Physics (CCEPP); Joint Large-Scale Scientific Facility Funds of the NSFC and CAS under Contracts Nos. U1332201, U1532257, U1532258; CAS Key Research Program of Frontier Sciences under Contracts Nos. QYZDJ-SSW-SLH003, QYZDJ-SSW-SLH040; 100 Talents Program of CAS; National 1000 Talents Program of China; INPAC and Shanghai Key Laboratory for Particle Physics and Cosmology; German Research Foundation DFG under Contracts Nos. Collaborative Research Center CRC 1044, FOR 2359; Istituto Nazionale di Fisica Nucleare, Italy; Koninklijke Nederlandse Akademie van Wetenschappen (KNAW) under Contract No. 530-4CDP03; Ministry of Development of Turkey under Contract No. DPT2006K-120470; National Natural Science Foundation of China (NSFC) under Contracts Nos. 11505034, 11575077; National Science and Technology fund; The Swedish Research Council; U. S. Department of Energy under Contracts Nos. DE-FG02-05ER41374, DE-SC-0010118, DE-SC-0010504, DE-SC-0012069; University of Groningen (RuG) and the Helmholtzzentrum fuer Schwerionenforschung GmbH (GSI), Darmstadt; WCU Program of National Research Foundation of Korea under Contract No. R32-2008-000-10155-0

---

[1] B. Aubert *et al.* (BABAR Collaboration), Phys. Rev. D. **74**, 091103(R) (2006).
[2] M. Ablikim *et al.* (BESII Collaboration), Phys. Rev. Lett. **100**, 102003 (2008).
[3] M. Ablikim *et al.* (BESIII Collaboration), Phys. Rev. D. **91**, 052017 (2015).
[4] C. P. Shen *et al.* (BELLE Collaboration), Phys. Rev. D. **80**, 031101(R) (2009).
[5] T. E. Coan *et al.*, (CLEO Collaboration), Phys. Rev. Lett. **96**, 162003 (2006).
[6] Gui-Jun Ding and Mu-lin Yan, Phys. Lett. B. **650**, 390 (2007).
[7] Gui-Jun Ding and Mu-lin Yan, Phys. Lett. B. **657**, 49 (2007).
[8] Zhi-Gang Wang, Nucl. Phys. **A791**, 106 (2007).
[9] Hua-Xing Chen, Xiang Liu, Atsushi Hosaka, and Shi-Lin Zhu, Phys. Rev. D. **78**, 034012 (2008).
[10] E. Klempt and A. Zaitsev, Phys. Rep. **454**, 1 (2007).
[11] F.E. Close, Phys. Lett. B342(1995)369;
F.E. Close, et al., Phys, Rev.D 57(1998)5653;
F.E. Close, S.Godfrey, Phys. Lett. B574(2003)210.
[12] K. A. Olive *et al.* (Particle Data Group), Chin. Phys. C **38**, 090001 (2014).
[13] A. Martinez Torres, K. P. Khemchandani, L. S. Geng, M. Napsuciale, and E. Oset, Phys. Rev. D. **86**, 074031(2008).
[14] B. Aubert *et al.* (BABAR Collaboration), Phys. Rev. D. **71**, 052001.
[15] B. Aubert *et al.* (BABAR Collaboration), Phys. Rev. D. **86**, 012008 (2012).
[16] A. Martinez Torres, K. P. Khemchandani, L. S. Geng, M. Napsuciale, and E. Oset, Phys. Rev. D. **78**, 074031 (2008).
[17] M. Ablikim *et al.* (BESIII Collaboration), Nucl. Instrum. Meth. A **614**, 345 (2010)
[18] Giovanni Balossini, Carlo M Carloni calame, Guido Montagna, Oreste Nicrosiniand Fulvio Phiccinini, $Nucl.Phys.B758, 227(2006)$.
[19] R. G. Ping, Chin. Pays. C, **38**, 083001(2014).
[20] E. A. Kuraev and V. S. Fadin, Yad. Fiz. **41**, 733 (1985).
[21] S. Actis et al., Eur. Phys. J. C **66**, 585 (2010).
[22] F.V. Hippel and C. Quigg, Phys. Rev. D. **5**, 624 (1972).
[23] M. Ablikim *et al.* (BESIII Collaboration), Phys. Rev. D. **83**,112005 (2011).
[24] M. Ablikim *et al.* (BESIII Collaboration), Chin. Pays. C, **41** (6), 063001(2017).
[25] D. Liu *et al.* (BESIII Collaboration), internal document.
[26] M. Ablikim *et al.* (BESIII Collaboration), Phys. Rev. D. **87**, 012002 (2013)